Experimental Observations

Some of the early (and classic) observations of individual traveling cavitation bubbles by Knapp and Hollander (1948), Parkin (1952), and Ellis (1952) make mention of the deformation of the bubbles by the flow. But the focus of attention soon shifted to the easier observations of the dynamics of individual bubbles in quiescent liquid, and it is only recently that investigations of the deformation caused by the flow have resumed. Both Knapp and Hollander (1948) and Parkin (1952) observed that almost all cavitation bubbles are closer to hemispherical than spherical and that they appear to be separated from the solid surface by a thin film of liquid. Such bubbles are clearly evident in other photographs of traveling cavitation bubbles on a hydrofoil such as those of Blake et al. (1977) or Briançon-Marjollet et al. (1990).

A number of recent research efforts have focused on these bubble/flow interactions, including the work
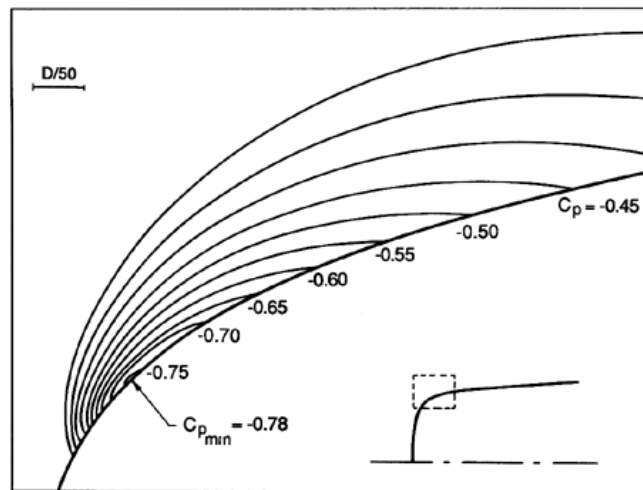

Figure 1: Isobars in the vicinity of the minimum pressure point on the axisymmetric Schiebe headform with values of the pressure coefficient, C_p, as indicated. The pressures were obtained from a potential flow calculation. The insert shows the headform shape and the area that has been enlarged in the main figure (dashed lines). From Schiebe (1972) and Kuhn de Chizelle et al. (1992b).

of van der Meulen and van Renesse (1989) and Briançon-Marjollet et al. (1990). Recently, Ceccio and Brennen (1991) and Kuhn de Chizelle et al. (1992a,b) have made an extended series of observations of cavitation bubbles in the flow around axisymmetric bodies, including studies of the scaling of the phenomena. Two axisymmetric body shapes were used, both of which have been employed in previous cavitation investigations. The first of these was a so-called "Schiebe body" (Schiebe 1972) which is one of a series based on the solutions for the potential flow generated by a normal source disk (Weinstein 1948) and first suggested for use in cavitation experiments by Van Tuyl (1950). One of the important characteristics of this shape is that the boundary layer does not separate in the region of low pressure within which cavitation bubbles occur. The second body had the ITTC headform shape originally used by Lindgren and Johnsson (1966) for the comparative experiments on cavitation inception. This headform exhibits laminar separation within the region in which the cavitation bubbles occur. For both headforms, the isobars in the neighborhood of the minimum pressure point exhibit a large pressure gradient normal to the surface, as illustrated by the isobars for the Schiebe body shown in Figure 1. This pressure gradient is associated with the curvature of the body and therefore the streamlines in the vicinity of the minimum

pressure point. Consequently, at a given cavitation number, σ, the region below the vapor pressure that is enclosed between the solid surface and the $C_p = -\sigma$ isobaric surface is long and thin compared with the size of the headform. Only nuclei that pass through this thin volume will cavitate.
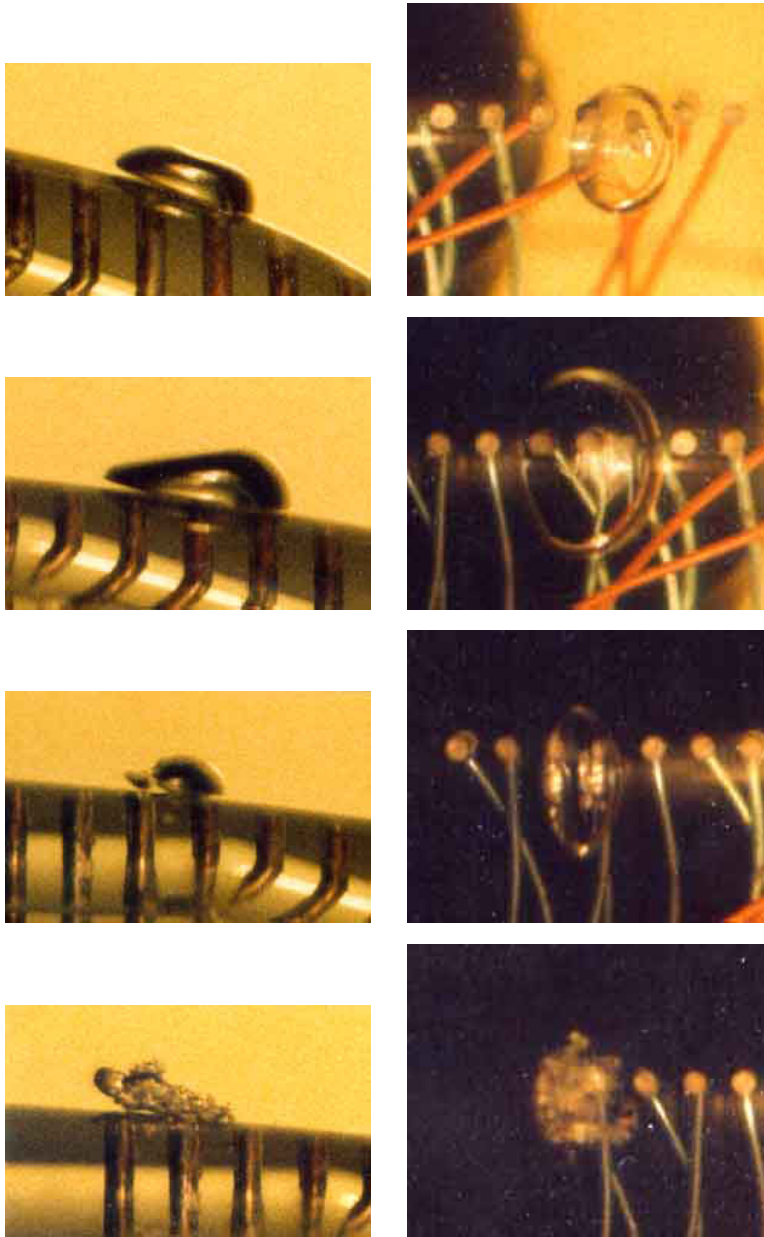

Figure 2: A series of photographs illustrating the growth and collapse of traveling cavitation bubbles in a flow around a 5.08 cm diameter Schiebe headform at $\sigma = 0.45$ and a speed of 9 m/s. Simultaneous profile and plan views are presented but each row is, in fact, a different bubble. The flow is from right to left. The scale is 4.5 times lifesize. From Ceccio and Brennen (1991).

The observations of Ceccio and Brennen (1991) at lower Reynolds numbers will be described first. Typical photographs of bubbles on the 5.08 cm diameter Schiebe headform during the cycle of bubble growth and collapse are shown in Figure 2. Simultaneous profile and plan views provide a more complete picture of the bubble geometry. In all cases the shape during the initial growth phase was that of a spherical cap, the bubble being separated from the wall by a thin layer of liquid of the same order of magnitude as the boundary layer thickness. Later developments depend on the geometry of the headform and the Reynolds

number, so we begin with the simplest case, that of the Schiebe body at relatively low Reynolds number. Typical photographs for this case are included in Figure 2. As the bubble begins to enter the region of adverse pressure gradient, the exterior frontal surface begins to be pushed inward, causing the profile of the bubble to appear wedge-like. Thus the collapse is initiated on the exterior frontal surface of the bubble, and this often leads to the bubble fissioning into forward and aft bubbles as seen in Figure 2.

Two other processes are occuring at the same time. First, the streamwise thickness of the bubble decreases faster than its spanwise breadth (spanwise being defined as the direction parallel to the headform surface and normal to the oncoming stream), so that the largest dimension of the bubble is its spanwise breadth. Second, the bubble acquires significant spanwise vorticity through its interactions with the boundary layer during the growth phase. Consequently, as the collapse proceeds, this vorticity is concentrated and the bubble evolves into one (or two or possibly more) cavitating vortex with a spanwise axis. These vortex bubbles proceed to collapse and seem to rebound as a cloud of much smaller bubbles. Often a coherent second collapse of this cloud was observed when the bubbles were not too scattered by the flow. Ceccio and Brennen (1991) (see also Kumar and Brennen 1993) conclude that the flow-induced fission prior to collapse can have a substantial effect on the noise impulse (see section (Nhg)).
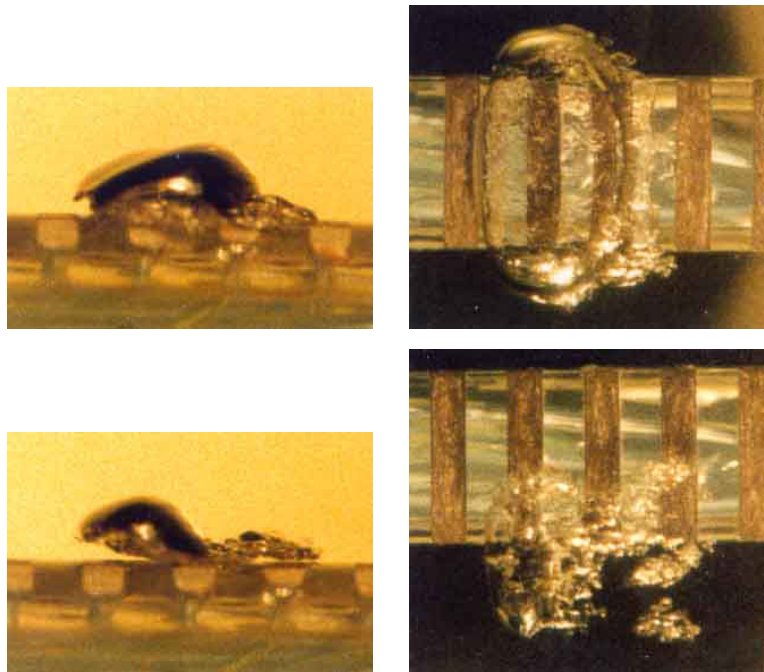

Figure 3: Examples of simultaneous profile and plan views illustrating the instability of the liquid layer under a traveling cavitation bubble. From Ceccio and Brennen (1991) experiments with a 5.08 cm diameter ITTC headform at $\sigma = 0.45$ and a speed of 8.7 m/s. The flow is from right to left and the scale is 3.8 times lifesize.

Two additional phenomena were observed on the ITTC headform, which exhibited laminar separation. The first of these was the observation that the layer of liquid underneath the bubble would become disrupted by some instability. As seen in Figure 3, this results in a bubbly layer of fluid that subsequently gets left behind the main bubble. Thus the instability of the liquid layer leads to another process of bubble fission. Because of the physical separation, the bubbly layer would collapse after the main body of the bubble.

The second and perhaps more consequential phenomenon observed with the ITTC headform only occurs with the occasional bubble. Infrequently, when a bubble passes the point of laminar separation, it triggers the formation of local "attached cavitation" streaks at the lateral or spanwise extremities of the bubble, as seen in Figure 4. Then, as the main bubble proceeds downstream, these "streaks" or "tails" of attached
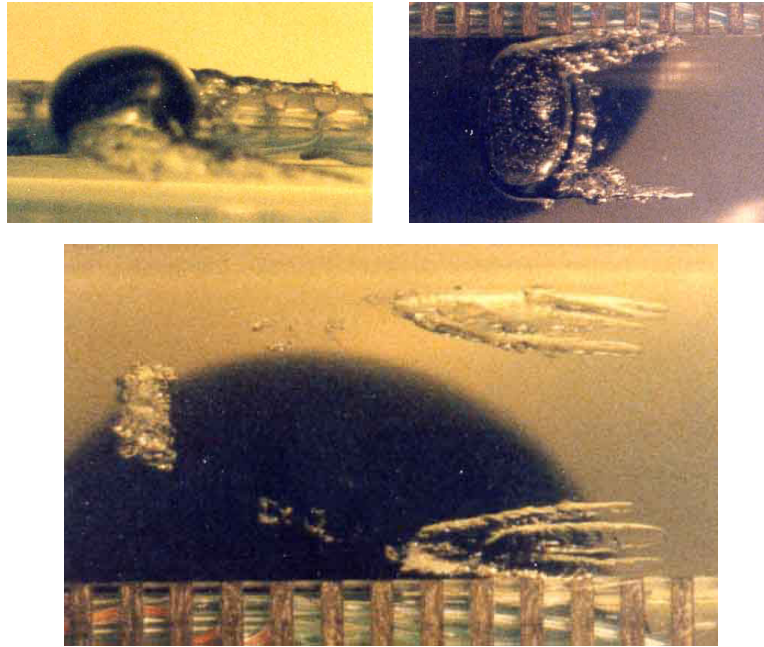
Figure 4: Examples illustrating the attached tails formed behind a traveling cavitation bubble. The top two are simultaneous profile and plan views. The bottom shows the persistence of the tails after the bubble has collapsed. From Ceccio and Brennen (1991) experiments with a 5.08 cm diameter ITTC headform at $\sigma = 0.42$ and a speed of 9 m/s. The flow is from right to left and the scale is 3.8 times lifesize.

cavitation are stretched out behind the main bubble, the trailing ends of the tails being attached to the solid surface. Subsequently, the main bubble collapses first, leaving the "tails" to persist for a fraction longer, as illustrated by the lower photograph in Figure 4.

The importance of these occasional "events with tails" did not become clear until tests were conducted at much higher Reynolds numbers, with larger headforms (up to 50.5 cm in diameter) and somewhat higher speeds (up to 15 m/s). These tests were part of an investigation of the scaling of the bubble dynamic phenomena described above (Kuhn de Chizelle et al. 1992a,b). One notable observation was the presence of a "dimple" on the exterior surface of all the individual traveling bubbles; examples of this dimple are included in Figure 5. They are not the precursor to a reentrant jet, for the dimple seems to be relatively stable during most of the collapse process. More importantly, it was observed that, at higher Reynolds number, "attached tails" occurred even on these Schiebe bodies, which did not normally exhibit laminar separation. Moreover, the probability of occurence of attached tails increased as the Reynolds number increased and the attached cavitation began to be more extensive. As the Reynolds number increased further, the bubbles would tend to trigger attached cavities over the entire wake of the bubble as seen in the lower two photographs in Figure 5. Moreover, the attached cavitation would tend to remain for a longer period after the main bubble had disappeared. Eventually, at the highest Reynolds numbers tested, it appeared that the passage of a single bubble was sufficient to trigger a "patch" of attached cavitation (Figure 5, bottom), which would persist for an extended period after the bubble had long disappeared. This progression of events and the changes in the probabilities of the different kinds of events with Reynolds number imply a rich complexity in the micro-fluidmechanics of cavitation bubbles, much of which remains to be understood. Its importance lies in the fact that these different types of events cause differences in the collapse process which, in turn, alters the noise produced (see Kuhn de Chizelle et al. 1992b) and, in all probability, the potential for cavitation damage. For example, the events with attached tails were found to produce significantly less noise than the events without tails. Due to the changes in the probabilities of occurence of these events with Reynolds number, this implies a scaling effect that had not been previously
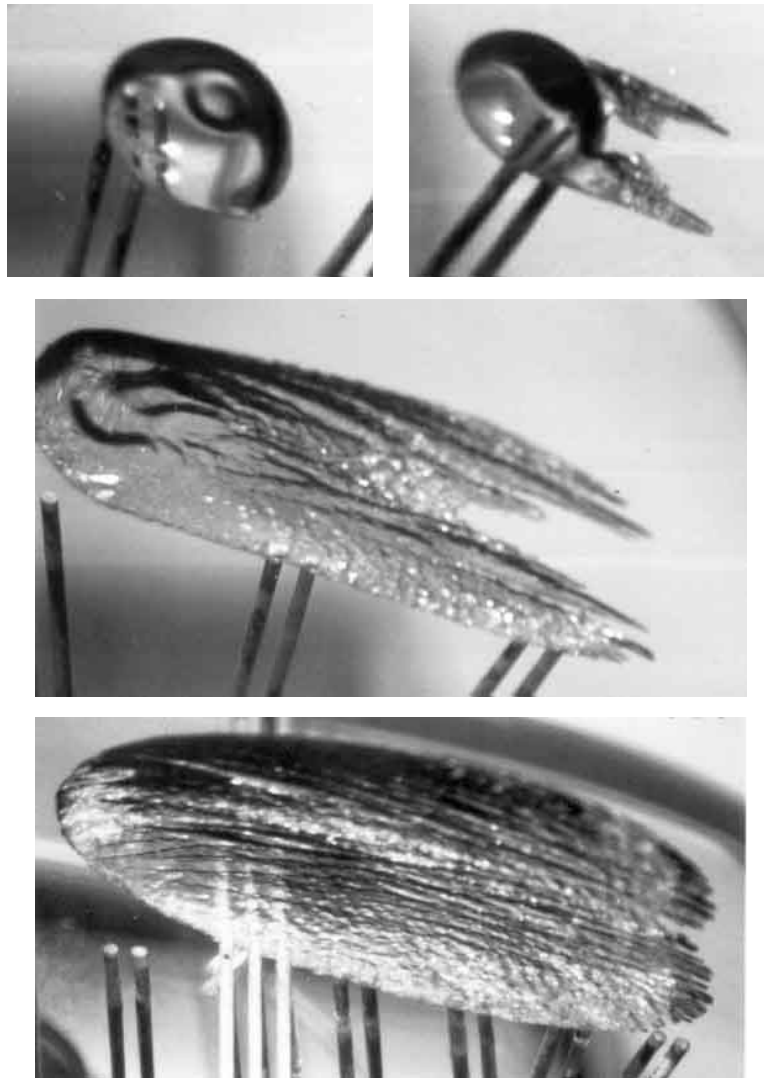
Figure 5: Typical cavitation events from the scaling experiments of Kuhn de Chizelle et al. (1992b) showing an unattached bubble with "dimple"(upper left), a bubble with attached tails (upper right), and a transient bubble-induced patch (middle), all occurring on the 50.8 cm diameter Schiebe headform at $\sigma = 0.605$ and a speed of 15 m/s. The bottom photograph shows a patch on the 25.4 cm headform at $\sigma = 0.53$ and a speed of 15 m/s. The flow is from right to left. The top three are shown at 1.3 times lifesize and the bottom at 1.25 times lifesize.

recognized. It also suggests some possible strategies for the reduction of cavitation noise and damage.

When examined in retrospect, one can identify many of these phenomena in earlier photographic observations, including the pioneering, high-speed movies taken by Knapp. As previously noted, Knapp and Hollander (1948), Parkin (1952), and others noted the spherical-cap shape of most traveling cavitation bubbles. The ITTC experiments (Lindgren and Johnsson 1966) emphasized the diversity in the kinds of cavitation events that could occur on a given body, and later authors attempted to identify, understand, and classify this spectrum of events. For example, Holl and Carroll (1979) observed a variety of different types of cavitation events on axisymmetric bodies and remarked that both traveling and attached cavitation "patches" occurred and could be distinguished from traveling bubble cavitation. A similar study of the different types of cavitation events was reported by Huang (1979), whose "spots" are synonymous with "patches."